Technical Note

Study of Variation in Dose Calculation Accuracy Between kV Cone-Beam Computed Tomography and kV fan-Beam Computed Tomography

Venkatesan Kaliyaperumal, C. Jomon Raphael, K. Mathew Varghese, Paul Gopu, S. Sivakumar, Minu Boban, N. Arunai Nambi Raj[1], K. Senthilnathan[2], P. Ramesh Babu[2]

Department of Radiation Oncology, Amala Institute of Medical Sciences, Thrissur, Kerala, [1]Centre for Biomaterials, Cellular and Molecular Theranostics, VIT University, [2]Department of Physics, School of Advanced Sciences VIT University, Vellore, Tamil Nadu, India

Abstract

Cone-beam computed tomography (CBCT) images are presently used for geometric verification for daily patient positioning. In this work, we have compared the images of CBCT with the images of conventional fan beam CT (FBCT) in terms of image quality and Hounsfield units (HUs). We also compared the dose calculated using CBCT with that of FBCT. Homogenous RW3 plates and Catphan phantom were scanned by FBCT and CBCT. In RW3 and Catphan phantom, percentage depth dose (PDD), profiles, isodose distributions (for intensity modulated radiotherapy plans), and calculated dose volume histograms were compared. The HU difference was within ± 20 HU (central region) and ± 30 HU (peripheral region) for homogeneous RW3 plates. In the Catphan phantom, the difference in HU was ± 20 HU in the central area and peripheral areas. The HU differences were within ± 30 HU for all HU ranges starting from −1000 to 990 in phantom and patient images. In treatment plans done with simple symmetric and asymmetric fields, dose difference (DD) between CBCT plan and FBCT plan was within 1.2% for both phantoms. In intensity modulated radiotherapy (IMRT) treatment plans, for different target volumes, the difference was <2%. This feasibility study investigated HU variation and dose calculation accuracy between FBCT and CBCT based planning and has validated inverse planning algorithms with CBCT. In our study, we observed a larger deviation of HU values in the peripheral region compared to the central region. This is due to the ring artifact and scatter contribution which may prevent the use of CBCT as the primary imaging modality for radiotherapy treatment planning. The reconstruction algorithm needs to be modified further for improving the image quality and accuracy in HU values. However, our study with TG-119 and intensity modulated radiotherapy test targets shows that CBCT can be used for adaptive replanning as the recalculation of dose with the anisotropic analytical algorithm is in full accord with conventional planning CT except in the build-up regions. Patient images with CBCT have to be carefully analyzed for any artifacts before using them for such dose calculations.

Keywords: Cone-beam computed tomography, dose calculation, fan-beam computed tomography, quality assurance

INTRODUCTION

Cone-beam computed tomography (CBCT) is an online three-dimensional (3D) imaging which is available for performing the daily patient positioning and analyzing the anatomical variation during radiotherapy.[1-3] For dose escalation in head and prostate cases, the image guidance is mandatory to achieve higher tumor control and to reduce normal tissue toxicity.[4,5] Once the volumetric information of the patient is obtained, the same can be used for recalculation of delivered dose on a daily basis and to verify it with the planned dose.[6] During radiotherapy in conformal treatment, tumor shrinkage and anatomical changes can affect the accuracy of dose delivery to the patient which has to be corrected by a new treatment plan with repeat CT.[7] Repeat fan beam CT imaging is used for re-planning, adequate dose coverage in planning tumor volume (PTV) and dose reduction to normal tissues for selected patients.[8]

Address for correspondence: Dr. P. Ramesh Babu, Department of Physics, School of Advanced Sciences, VIT University, Vellore - 632 014, Tamil Nadu, India. E-mail: prameshbabu@vit.ac.in

Access this article online

Quick Response Code:

Website:
www.jmp.org.in

DOI:
10.4103/jmp.JMP_24_17

How to cite this article: Kaliyaperumal V, Raphael CJ, Varghese KM, Gopu P, Sivakumar S, Boban M, et al. Study of variation in dose calculation accuracy between kV cone-beam computed tomography and kV fan-Beam computed tomography. J Med Phys 2017;42:171-80.

Several studies have been published about Hounsfield unit (HU) validation and use of CBCT for adaptive radiotherapy (ART). Ping and Kandaiya[9] studied about the HU value changes in CBCT due to patient geometry and size. In this study, it was mentioned that independent HU-electron density mapping was needed for different volumes. Mao *et al*.[10] studied online dosimetric evaluation of larynx stereotactic body radiotherapy. Boggula *et al*.[11] discussed about online adaptive planning using CBCT in prostate cases and stated that accurate dose calculations were possible if the CBCT images were correlated for density distributions. Søvik *et al*.[12] evaluated the ART using contrast-enhanced CBCT (CECBCT) and concluded that the non-adaptive strategy was inferior when compared with CECBCT-based adaptive planning.

Bertelsen *et al*.[13] evaluated the CBCT for biological ART in lung cases and had shown that density changes in CBCT correlated with clinical toxicities. Kibrom and Knight[14] used the CBCT scans for ART in bladder cancer where daily re-optimization plans were found to be superior than the original plan. Zhang *et al*.[15] studied the CBCT dose validation for nasopharyngeal carcinomas and showed the calculation difference was <2% when compared with fan beam-computed tomography (FBCT) dose calculation. The above study mandates that the HU-electron density correction has to be applied for accurate dose calculations.

Yang *et al*.[16] studied the HU variation and dose calculation between FBCT and CBCT. They showed that static CBCT scans could be used for dose calculation purposes, provided corresponding electron density data were available. The work was carried out with Catphan, CIRS phantom, and few clinical cases (head and neck, thorax, and pelvis). Ding *et al*.[17] discussed about CBCT images for adaptive planning. In this study, it was found that CBCT images could be used for dose planning while the HU deviation was irrelevant.

In our work, we investigated the CBCT image quality and the feasibility of using these images for dose calculations in phantoms and patients for ART. In the previous works discussed above, to the best of our knowledge, all the authors have studied the dose calculations with simple targets in the phantoms. However, we have used the structure sets of target and normal tissue similar to that of TG 119[18] which are of different types and complexities covering the entire volume of the phantom. We have also used clinical implementation of intensity modulated radiotherapy (IMRT) guide[19] to study whether the CBCT images can be taken as primary imaging modality for inverse optimization. For this, image quality assurance was performed to determine whether the CBCT images have similar image quality as FBCT images. Relative electron density calibration was carried out and values were fitted with treatment planning system (TPS). The deviation of CT number and variation of dose calculation were compared between FBCT and CBCT. Dose calculation validation was performed in IMRT using homogenous (RW3 slab phantom) and inhomogeneous (Catphan 504) phantoms, and few clinical cases

with smaller target volumes (head and neck and pelvis cases). All the dose calculations were done with anisotropic analytical algorithm (AAA) for 6 MV and 15 MV photon beams.

METHODS AND MATERIALS

Imaging system
A Varian Clinac iX (Varian Oncology Systems, Palo Alto, CA, USA) medical linear accelerator having photon energies of 6 MV and 15 MV and electron energies of 6, 9, 12, and 15 MeV with On Board Imager (OBI) (version 1.5) having active detector area of 39.7 cm × 29.8 cm with a detector resolution of 1024 × 768 pixels was used in the study. The pixel size can be chosen between 0.488 mm to 1.953 mm for full fan mode (field of view [FOV] 25 cm × 25 cm) and in half fan mode (FOV 45 cm × 45 cm) from 0.8789 mm to 3.515 mm. This detector can provide 2-dimensional kV projection images and can reconstruct 3-dimensional images using Feldkamp *et al*. algorithm.[20] In this reconstruction, the attenuated values in the projections are convolved and back projected to create the image with Fourier transformations. The X-ray tube has a target angle of 14° with two focal spots (0.4 mm and 0.8 mm) available for acquiring the images. The maximum FOV is 25 cm × 25 cm for full fan and 45 cm × 45 cm for half fan with a length of 15 cm. The head acquisition mode (full fan) is used for head and neck and brain cases which have a small treatment area (<25 cm × 25 cm). For larger sites like pelvis, thoracic mode (half scan) was used (>25 cm × 25 cm). In full fan mode, the beam central axis passes through the detector center to take full projections. On the contrary, in half fan mode, the detector is shifted laterally to take only half of the projection of the scanned patient for each acquiring angle. In half fan, the total gantry rotation is 360° and in full fan mode, it is 200°.The number of projections is 655 and 360, for half and full fan modes respectively. FBCT imaging was done on a Siemens Sprit CT scanner with a gantry angle of 0°. The scanner has an ultrafast ceramic detector consisting of scintillation crystal lattice of a rare earth compound gadolinium oxysulfide. The image matrix was a 512 × 512 matrix, and the pixel value was 0.977 mm × 0.977 mm. In this study, all the phantoms and patients scans were taken at 2 mm slice thickness, both in CBCT and FBCT.

Quality assurance of cone-beam computed tomography and kV fan beam-computed tomography
The combined QA program consists of three parts, namely, safety and functionality, geometry, and image quality.[21] The OBI quality assurance was carried out routinely on a daily, weekly, and monthly basis. Daily checks were done which included tube warm-up, door interlock, and collision detections. The tube warm-up was recommended to prevent premature failure of the X-ray tube. In weekly checks, isocenter of the OBI was verified with 0°, 90°, 180°, and 270° gantry angles, and isocenter tolerance was <1.5 mm. Catphan 504 phantom (The Phantom Laboratory, Salem, NY, USA) with different modules was used in this study. HU linearity and spatial linearity were

assessed with CTP 404 consisting of air (75%N, 23.2%O, 1.3%A), PMP (C6H12 [CH2]), LDPE (C2H4), water (H$_2$O), polystyrene (C8H8), acrylic (C5H8O2), Delrin (proprietary), and Teflon (CF2) inserts. In this module, air and Teflon were placed 5 cm apart to measure the spatial linearity.

For low-contrast resolution, CTP 515 module was used, having different target diameters (2 mm to 15 mm) with a contrast of 0.3% to 1%. For high-contrast resolution, CTP 528 module was used having up to 21 line pairs per cm (starting from 1 lp/cm). For HU uniformity, CTP 486 module was used. The HU value should ideally be within 2% (20 HU) of water's density at standard scanning protocols and should typically record CT numbers ranging from 5 HU to 18 HU. This module was used for measurements of spatial uniformity, mean CT number, and noise value.[22]

Configuration of kV fan beam-computed tomography and cone-beam computed tomography in treatment planning system

CT number to electron density calibration curve for both the scanners need to be configured in TPS.[23,24] For this, CTP404 module of Catphan® phantom was used. HU electron density calibration for FBCT was done in the normal mode with 125 kVp and for CBCT, it was done with both half fan (125 kVp) and full fan mode (100 kVp).The CTP404 module has a diameter of 150 mm and a length of 16 cm. It contains 17 different sizes of inserts with seven different materials. Their relative electron densities range from 0 to 1.526. The region-of- interest (ROI) was selected for each material disk to cover a 3 mm × 3 mm square. The mean HU values in the ROIs were measured and HU electron density calibration curves were plotted with the relative electron density values. In TPS (Eclipse version 10), planning CT (FBCT) and CBCT were configured with separate CT calibration file for each scanner.

RW 3 plates and catphan phantom study

FBCT and CBCT images of the homogenous RW3® slab phantom (Polystyrene and TiO2 Doped plates of size 30 cm × 30 cm × 1 cm) and inhomogeneous Catphan® 504 phantom were acquired. The quoted density of RW3 phantom was 1.045 g/cc, and its electron density was 1.012 times higher than the electron density of water. The image quality was analyzed for the homogenous RW3® slab phantom and Catphan® 504 phantom. HU distribution of all images in the central and the peripheral regions of the phantom were quantified.

Treatment plans with photons (energies 6 MV and 15 MV) of open and wedged fields (15°, 30°, 45°, and 60°) with different symmetric (4 cm × 4 cm, to 12 cm × 12 cm) and asymmetric combinations were generated in images of both phantoms. Isodose profile, PDD, and dose at different depths were compared for the homogenous phantom. Various dummy contours of target and normal structures were drawn in Catphan® 504 phantom. Several target volumes such as shallow target, deep cylindrical target, C-shaped target, target in the buildup region and normal structures such as spinal cord were drawn [Figure 1]. IMRT plans

were also generated using an inverse planning algorithm (Helios VMS) to validate the CBCT in optimization algorithms. The basic intention was to simulate all possible criteria for simple and as well as complicated plans. For C-shaped target, the plan was done with 6 MV with gantry angles of 0°, 40°, 80°, 120°, 160°, 200°, 240°, 280°, 320,° (9 fields) and for buildup region target, the plan was done with 6 MV with gantry angles of 0°, 330°, 300°, 270°, 240°, and 210° (6 fields). For the simple cylindrical target, the planning was done with 9 fields of 15 MV and for the ring-shaped target, the planning was done with 18 fields equally spaced from 0° to 360° in steps of 20°. Dose calculation was performed with AAA with a grid size of 2 mm and with inhomogeneity correction.[25] Comparison of both plans was done using target dose homogeneity, conformity index, volume of PTV receiving the 95% of prescription dose (V95), percentage of prescription dose delivered to 95% volume of PTV (D95), maximum dose, and mean dose to normal structures. The maximum and mean dose to normal structures were expressed as percentage of prescription dose.

Target dose homogeneity index and conformity index were derived using the following formula.[26]

$$\text{Homogeneity index} = \frac{(D2\% - D98\%) \times 100}{D50\%} ----1$$

where D2%: Dose delivered to 2% target volume;

D98%: Dose delivered to 98% target volume;

D50%: Dose delivered to 50% target volume.

$$\text{Conformity index} = \frac{\text{Volume of body PD}}{\text{Volume of PTV PD}} -----2$$

where body PD: Volume of body receiving prescription dose (cc)

PTV PD: Volume of PTV receiving prescription dose (cc)

Using prediction dosimetry option in Varian Eclipse TPS, verification plans were created for kV FBCT and CBCT plans.
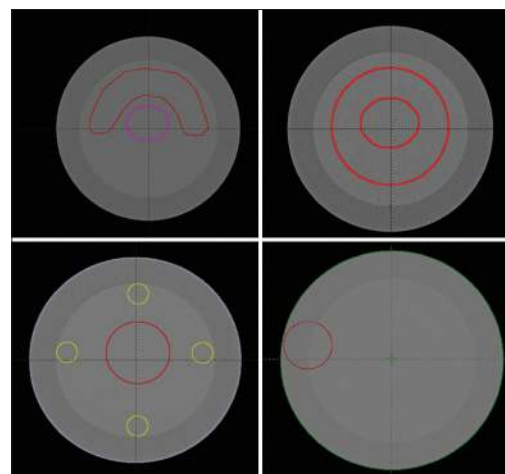

Figure 1: C-shaped, cylindrical, ring-shaped target, and target in buildup region in Catphan

Head and neck and pelvis case

Two patient data sets (one buccal mucosa case and one sacrum case) were selected for the analysis of dose calculation, and plans were generated using Helios optimization. For buccal mucosa patient, the plan was done with five 6 MV beams with the gantry angles of 350°, 30°, 70°, 100°, 135°. In the sacrum (pelvis), the plan was done with 15 MV beams with the gantry angles of 75°, 135°, 180°, 225°, 285°. The patient specific QA was performed by point dose measurement and 2D fluence verification using 0.125 cc (PTW) chamber and portal prediction dosimetry system, respectively. On the day of implementation, isocenter verification was done with 2D kV orthogonal images. The actual treatment couch parameters (lateral, longitudinal, and vertical) were acquired for further daily treatments, and the patient's position was confirmed with online 3D volumetric imaging. In TPS, structure sets from kV FBCT were transferred to registered CBCT image set. The dose calculation was performed on the CBCT image set, with the same fluence, MU, and same configuration (except electron density calibration) which were used earlier in kV FBCT. The dose distributions were compared by isodose color wash. The two-dimensional pictorial graph from 3D volumetric dose volume histograms (DVH) were analyzed for PTV, CTV, and normal organs.

RESULTS

Quality assurance of fan beam-computed tomography and cone-beam computed tomography

The CBCT isocenter verification performed weekly as per department protocol was <1 mm. Images of different modules in Catphan 504 phantom showed that the HU linearity (tolerance is <40 HU), low-contrast resolution (tolerance is 4th disk [7 mm dia]), and high-contrast resolution (spatial resolution-tolerance is group 6 i.e., 6 lp/cm), spatial linearity (tolerance is $<\pm1$ mm), and HU uniformity (tolerance is <40 HU) for both FBCT and CBCT were <40 HU [Figure 2a]. HU values for both images from air to Teflon were within acceptable limits ($<\pm40$ HU from the given value). CTP 515 module in Catphan 504 phantom was used to verify the low-contrast resolution, and it had supra-slice and sub-slice contrast targets. The targets have contrast levels of 0.3%, 0.5%, and 1%. The tolerance level is a visualization of 7 mm diameter disk (4th disk from the bigger one). The average of the measurements was made
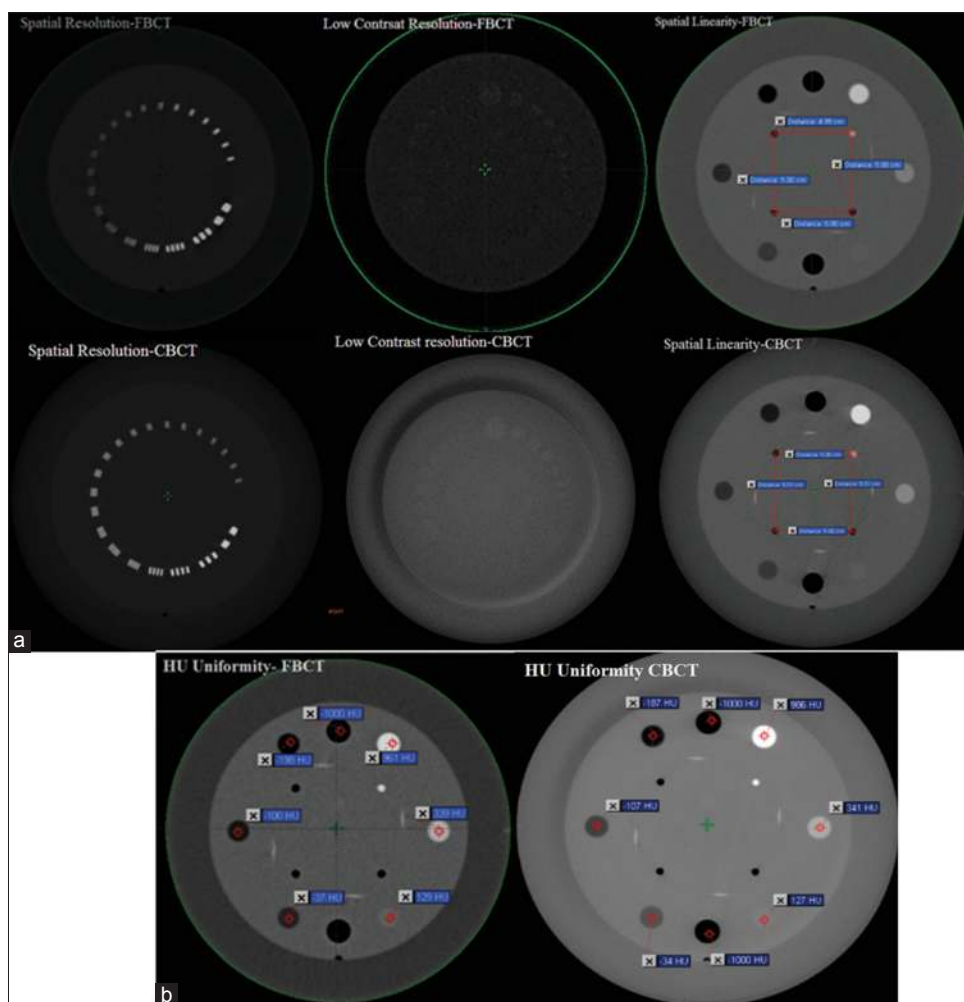

Figure 2: (a) High-contrast resolution, low-contrast resolution, spatial linearity of fan beam-computed tomography and cone-beam computed tomography images. (b) Hounsfield unit comparison of fan beam-computed tomography and cone-beam computed tomography images

from several scans to check the imaging consistency. FBCT and CBCT low-contrast and spatial resolution over a period of three years were found to be within tolerance levels as studied by Yoo *et al.*[21] For high-contrast resolution, CTP528 module was used. It has 21 line pairs/centimeter (lp/cm) gauges. The resolution was determined by the number of line pairs one could visualize out of the 21 line pairs gauge and accordingly a score between 1 and 21 was recorded. The tolerance is a visualization of 6 lp/cm. CTP 486 module for image uniformity is cast from a uniform material. The material has HU value from 5 to 18. Mean CT numbers within an ROI of 1 cm × 1 cm in center and peripheral region were obtained with their corresponding standard deviation and noise value. The spatial uniformity (HU uniformity) was within ± 20 HU for both image sets.

Configuration of fan beam-computed tomography and cone-beam computed tomography scanner in treatment planning system

Catphan 504 phantom was used to generate CT electron density calibration curves for the CT scanner and CBCT [Figure 2b]. Table 1 shows the estimated electron density, estimated and measured HU values and calculated relative electron density for different mediums. The half fan mode was used

for calibration, and the procedure was repeated in full fan mode also. No major HU deviation was found (<40 HU) in the uniform region of Catphan phantom. CBCT imaging was repeated over a month for full fan and half fan acquisition modes to verify the HU stability. The CT number was taken between the air (-1000) and Teflon (990). For deriving electron density relative to the electron density of water, the ICRU report 42[27] was used (Equation 3 and 4).

$$\rho^{\omega, e} = 1{,}0 + 0{,}001 \times N_{CT} - 1000 \leq N_{CT} \leq 100 \quad ------3$$

$$\rho^{\omega, e} = 1{,}052 + 0{,}00048 \times N_{CT} \quad N_{CT} > 100 \quad ------4$$

Here, $\rho^{\omega, \varepsilon}$ - relative electron density to water

N_{CT} - CT number (HU)

The two modalities were compared and minimal deviation was found in HU (<40 HU) value, and half fan mode was taken as a reference.

RW 3 plates and Catphan comparison
Hounsfield unit comparison
Variation in the HU values of homogenous RW3 plates was within ± 20 HU in the central region [Figure 3a]. Due to ring

Table 1: Relative electron density values for fan beam computed tomography and cone-beam computed tomography (CTP404 module) (half fan and full fan)

Material	Electron density (×10²³ e/g)	HU (estimated)	HU_FBCT	HU_CBCT (HF)	HU_CBCT (FF)	RED_FBCT	RED_CBCT	RED_CBCT (FF)
Air	3.007	−1000	−1000	−1000	−999.4	0	0	0.0006
PMP	3.435	−200	−198	−187	−190.3	0.802	0.813	0.8097
LDPE	3.429	−100	−100	−107	−117	0.9	0.893	0.883
Polystyrene	3.238	−35	−37	−34	−13.7	0.963	0.966	0.986
Water	3.343	0	2	0	7	1.002	1	1.007
Acrylic	3.248	120	121	127	156.9	1.11	1.113	1.127
Delrin	3.209	340	339	341	360.4	1.215	1.216	1.225
Teflon	2.889	990	961	986	1023.1	1.513	1.525	1.543

HU: Hounsfield units, FB: Fan beam, CBCT: Cone-beam computed tomography, HF: Half fan, FF: Full fan, PMP: Polymethylpentene, LDPE: Low-density polyethylene, RED: Relative electron density
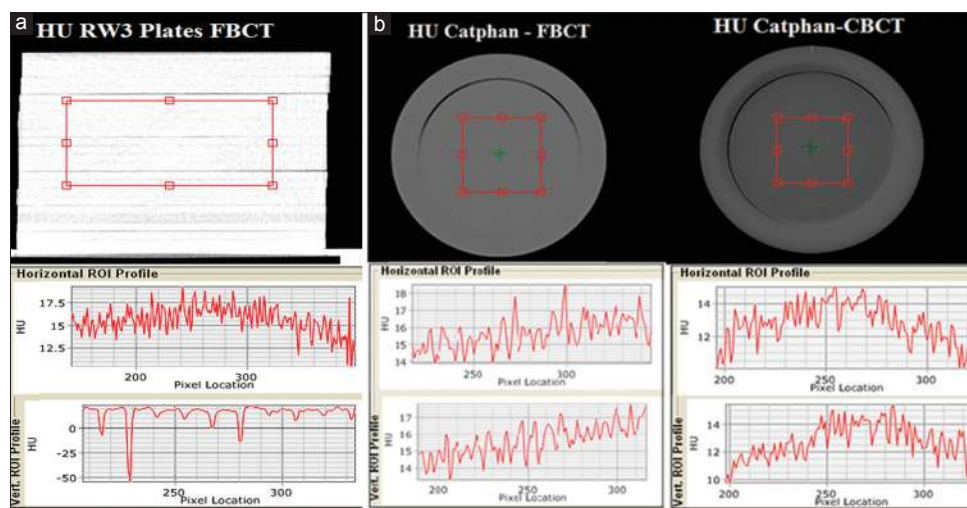

Figure 3: (a) Hounsfield unit value in X and Z axis fan beam-computed tomography versus cone-beam computed tomography RW Plates. (b) Hounsfield unit value in X and Z axis fan beam-computed tomography versus cone-beam computed tomography - Catphan phantom

artifact, the difference was more in the peripheral region and was within ± 30 HU. The mean values were 15.6 HU and 19.1 HU over the ROI of 256 mm × 128 mm for FBCT and CBCT respectively and their standard deviations were 3.69 HU and 5.01 HU. In CTP 486 module of Catphan 504 phantom, the HU uniformity with CBCT image was within ± 10 HU over the region of 129 mm × 129 mm in comparison with FBCT image [Figure 3b]. The mean HU value was 15.7 HU and 12.8 HU for FBCT and CBCT respectively, and their standard deviation was 3.96 HU and 4.79 HU. The variation between FBCT and CBCT with both half fan and full fan mode for different materials having HU values ranging from −1000 to 990 was < ±40 HU.

The white ring was observed in CBCT images for both half fan and full fan mode while changing the grayscale from −885 HU to 1330 HU for half fan and -804 to 1715 HU for full fan.

Dose comparison

In uniform RW3 plates, the dose deviation between FBCT and CBCT plans for different points was within ± 1% in symmetric field (10 cm × 10 cm) and within ± 1.2% in asymmetric fields except in the buildup region (for 6 MV <1 cm and for 15 MV <2.5 cm) [Table 2]. For wedged fields, the variation was within 1%. In Catphan phantom, the above plans were done on FBCT and CBCT. The dose deviation in different points was < 1% for both symmetric and asymmetric fields in the uniform area (CTP 486 module) except in the build-up region [Table 2]. For wedged fields, the deviation was <1.5% for both 6 MV and 15 MV.

In C-shaped target, D95 for the target was 94.5% and 95.7% for plans done on FBCT and CBCT respectively [Figure 4a and c]. Maximum dose to normal structure was 59.5% and 61.6% of target prescription dose and the mean dose was 31.7% and 32.1% for FBCT and CBCT plans respectively. For ring-shaped target [Figure 4b and c], D95 for the PTV was 96.02% and 96.16% for FBCT and CBCT plans respectively. The target coverage, (V95) was 99.8% for both FBCT and CBCT plans. V5 was 109.2% and 108.5% for

FBCT and CBCT plans, respectively. The central OAR mean dose was 75.1% (FBCT) and 74.9% (CBCT). In the buildup region, V95 for the PTV was 101.18% and 100.37% for FBCT and CBCT plans with a high homogeneity [Figure 5a and c]. V5 was 108.89% and 109.25% for FBCT and CBCT plans,
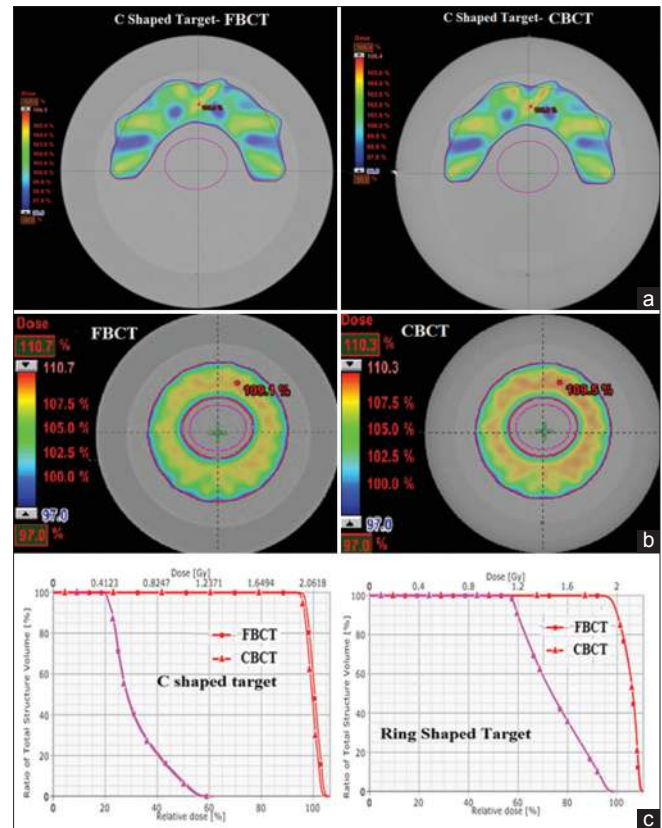

Figure 4: (a) Comparison of dose distribution between fan beam computed tomography and cone-beam computed tomography plans for C-shaped target. (b) Comparison of dose distribution between fan beam-computed tomography and cone-beam computed tomography plans for ring shaped target. (c) Comparison of dose volume histograms between fan beam-computed tomography and cone-beam computed tomography plans for C-shaped target and ring-shaped target

Table 2: Dose difference between fan beam computed tomography and cone-beam computed tomography plans at various depths

Depthcm in water	6 MV						15 MV					
	Dose in RW 3 plates Homogenous (Gy)			Dose in catphan phantom Nonhomogenous (Gy)			Dose in RW3 plates Homogenous (Gy)			Dose in catphan phantom Nonhomogenous (Gy)		
	FBCT	CBCT	Difference (%)	FBCT	CBCT	Difference (%)	FBCT	CBCT	Difference (%)	FBCT	CBCT	Difference (%)
1	1.098	1.082	1.46	1.093	1.097	−0.37	0.877	0.844	3.76	0.900	0.904	−0.44
1.5	1.125	1.124	0.09	1.115	1.112	0.27	0.987	0.966	2.13	0.994	0.996	−0.20
2	1.110	1.117	−0.63	1.100	1.096	0.36	1.038	1.031	0.67	1.040	1.041	−0.10
3	1.060	1.068	−0.75	1.051	1.046	0.48	1.059	1.066	−0.66	1.061	1.054	0.66
4	1.009	1.010	−0.10	0.988	0.982	0.61	1.039	1.043	−0.38	1.032	1.034	−0.19
5	0.954	0.956	−0.21	0.973	0.979	−0.62	0.992	0.999	−0.71	1.013	1.020	−0.69
10	0.724	0.720	0.55	0.719	0.713	0.83	0.785	0.784	0.13	0.795	0.794	0.13
12	0.645	0.640	0.78	0.640	0.634	0.94	0.713	0.716	−0.42	0.719	0.718	0.14

CBCT: Cone-beam computed tomography, FBCT: Fan beam computed tomography

respectively. For simple targets, D95 for the PTV was 98.4% and 92.6% for FBCT and CBCT plans. We found maximum deviation in the PTV coverage for this target because of four-sided uniform normal surrounding structures, but the OAR's dose was <1% [Figure 5b-c and Table 3]. Table 4 shows homogeneity and conformity index for different types of targets, and there is <1% deviation between FBCT and CBCT. Table 3 shows the normal structure doses for different types of target. For verifying the IMRT plans, the

Figure 5: (a) Comparison of fan beam-computed tomography and cone-beam computed tomography plans –Buildup region target. (b) Comparison of fan beam-computed tomography and cone-beam computed tomography plans -simple cylindrical target and 4 sides OAR (c) Comparison of dose volume histograms for fan-beam computed tomography and cone-beam computed tomography plans – Buildup region target and simple cylindrical target and 4 sides OAR

portal dosimetry option was used. In portal dosimetry, the 2D fluence of each field was verified between plans done on FBCT and CBCT. The predicted FBCT and CBCT IMRT plans were evaluated for gamma,[16] and the passing rate was more than 96% in all the plans (1 mm distance to agreement [DTA], 1% DD).

Head and neck and pelvis case
Hounsfield unit comparison
In bones, the deviation between the HU values was ± 20 HU with the mean value being 995 HU for FBCT images and 1005 HU for CBCT images over the central region of 16 mm × 16 mm with a standard deviation of 2.8 (FBCT) and 3.6 (CBCT). In soft tissues, the minimum HU value over the region of 15 mm × 15 mm was −63 (FBCT) and −96 (CBCT), and maximum HU value was 106 (FBCT) and 116 (CBCT). The mean HU value of soft tissue was −11.1 and −8.8 for FBCT and CBCT, respectively. The standard deviation was observed to be large (9.74 HU for FBCT and 10.86 HU for CBCT) because the ROI has more non-uniform HU values [Figure 6].

Dose comparison
The dose deviations for different points were <1% between the plans done on FBCT and CBCT images in all the IMRT plans. Figure 7 shows the dose color wash and DVH between the plans done on FBCT and CBCT. In the buccal mucosa case, the dose to 98% of PTV volume was 95.49% of prescription dose for FBCT plan and 96.38% for CBCT plan. In the sacrum case, the FBCT plan dose distribution was also comparable with CBCT plan [Figure 8]. The dose to 98% of PTV volume was 94.4% of prescription dose and for CBCT, it was 94.8%.

Discussion
Image quality and Hounsfield unit comparison
Several authors discussed the image quality of the CBCT in uniform as well as in inhomogeneous phantom.[28-33] In our study, the image quality was assessed with contrast resolution (low and high), spatial linearity and HU uniformity. In uniform phantom (RW3 plates), the HU value was comparable (variation is <20), and the noise in CBCT was more than that in FBCT. In the peripheral region of the phantom, HU values differed due to ring and streak artifacts.
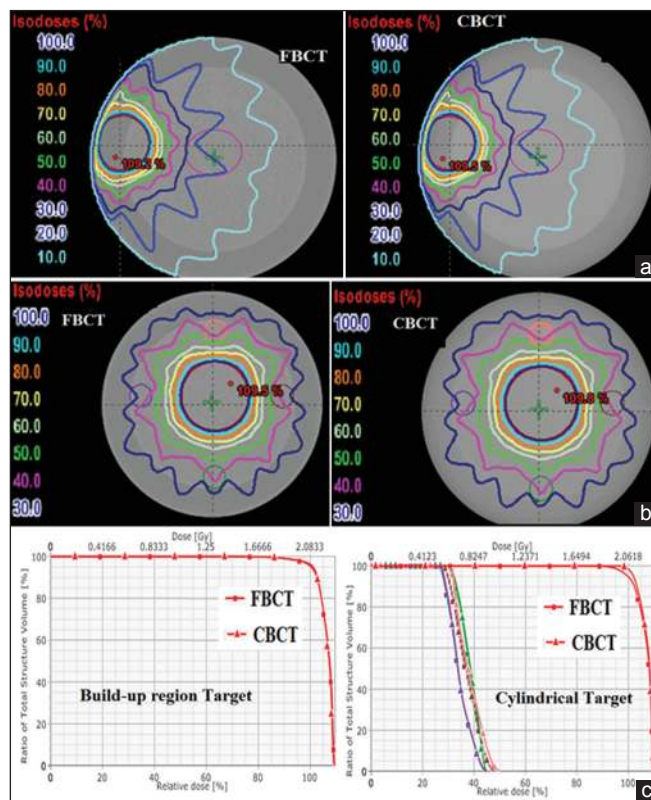
Table 3: Normal structure dose for the C-shaped, cylindrical, ring-shaped and build region fan beam computed tomography and cone-beam computed tomography plans

Target	NS	Max dose			Mean dose		
		FBCT	CBCT	Difference (%)	FBCT	CBCT	Difference (%)
C-shaped	NS 1	1.228	1.269	−3.34	0.653	0.661	−1.23
Cylindrical	NS 1	0.943	0.951	−0.85	0.828	0.825	0.36
	NS 2	1.018	1.019	−0.10	0.784	0.779	0.64
	NS 3	0.99	0.992	−0.20	0.775	0.77	0.65
	NS 4	0.934	0.941	−0.75	0.718	0.716	0.28
Ring shaped	NS 1	1.946	1.927	0.98	1.481	1.478	0.20
Buildup region	NS 1	0.627	0.624	0.48	0.27	0.271	−0.37

CBCT: Cone-beam computed tomography, FBCT: Fan beam computed tomography, NS: Normal structure

Table 4: Target dose homogeneity index and conformity index for C-shaped, cylindrical, ring shaped, and buildup region target in Catphan phantom - fan beam-computed tomography and cone-beam computed tomography plans

Target	C shaped			Cylindrical			Ring shaped			Buildup region		
	FBCT	CBCT	Difference (%)	FBCT	CBCT	Difference (%)	FBCT	CBCT	Difference (%)	FBCT	CBCT	Difference (%)
D 2% (Gy)	2.13	2.15	−0.94	2.20	2.20	−0.32	2.15	2.14	0.33	2.28	2.28	0.09
D 98% (Gy)	1.97	1.99	−1.27	2.07	2.02	2.42	1.95	1.94	0.26	2.00	1.99	0.80
HI	8.30	8.05	0.25	6.35	9.20	−2.85	10.15	10.05	0.1	13.86	14.56	−0.7
Volume (cc) of body$_{PD}$	486.05	500.14	−2.90	199.31	198.83	0.24	540.75	529.27	2.12	111.01	108.59	2.18
Volume (cc) of PTV$_{PD}$	440.66	435.31	1.21	178.82	181.32	−1.40	517.93	517.83	0.02	90.18	88.84	1.48
Conformity index	1.10	1.15	−0.046	1.12	1.10	0.018	1.04	1.02	0.022	1.23	1.22	0.009

PTV: Planning target volume, CBCT: Cone-beam computed tomography, FBCT: Fan beam-computed tomography, PD: Prescription dose, HI: Homogeneity index
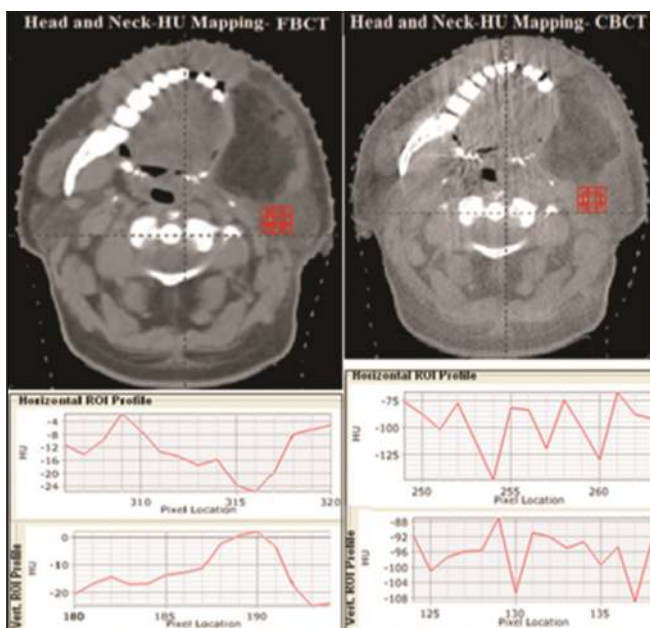

Figure 6: HU mapping in the ROI of 12 mm x 12 mm for head and neck case - FBCT and CBCT
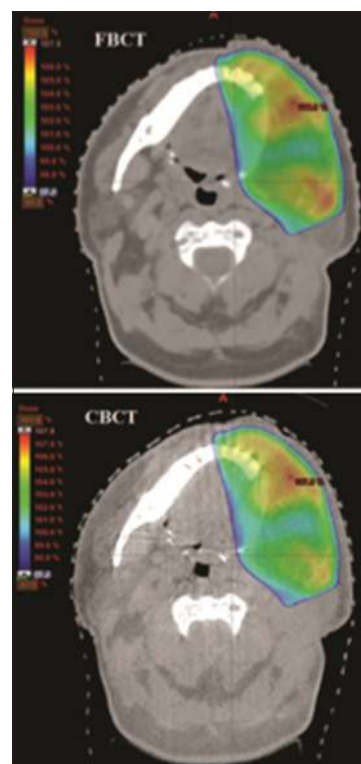

Figure 7: Dose comparison in the left buccal mucosa case- fan beam-computed tomography and cone-beam computed tomography - 6 MV

For overcoming this problem, Jin *et al.*[34] used an in-house partial reconstruction algorithm that reduced the scatter leading to reduced streak artifacts and improved image quality.

Niu *et al.*[35] showed how to reduce the CBCT dose as well as improve the image quality in C-arm using prior image constrained compress sensing algorithm.

Wang *et al.*[36] discussed the soft-tissue image quality to improve the contrast by reducing the noise with separable footprints with trapezoid functions technique. In inhomogenous phantom, the CBCT-contrast resolution, and spatial linearity were comparable with our planning FBCT images and within the acceptable criteria. In filtered images, pixel specific gain value correction factors (ratio of ideal to measured pixel values) can be used to reduce the ring artifact which was discussed by Altunbas *et al.*[37] Yang *et al.*[16] showed that in the static phantom scan, the variation in HU value was <10% and in our study, the variation was <10HU in the uniform region of CTP486 module

of the Catphan® phantom. In the inhomogeneous region, the difference was <25 HU, but over the ROI (3 mm × 3 mm) the difference was <10 HU. In patient (head and neck and pelvic case) scans, the differences in HU values were more (pixel to pixel based), but the deviation was less when we compared the HU values in the fixed ROI. Ding *et al.*[17] discussed the HU difference was higher in half fan mode; however, in our study the HU variations were less in half fan mode. High-resolution images are needed for delineating target and normal structures. The resolutions of commercially available CBCT scans are lesser when compared with the FBCT images, which may prevent the use of CBCT as the primary imaging modality for radiotherapy treatment planning. For adaptive replanning, the CBCT images can be used for assessing the target shrinkage or body mass reduction with suitable image registration, and
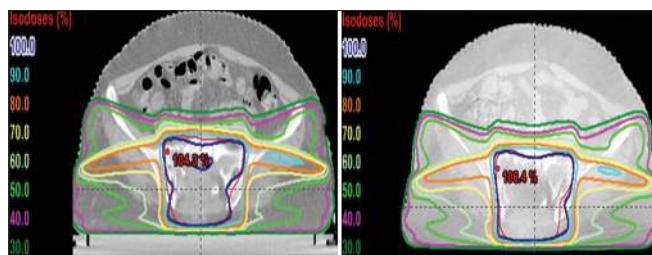
Figure 8: Dose comparison in the sacrum case- fan beam-computed tomography and cone-beam computed tomography - 15 MV

the structures can be propagated to CBCT from FBCT for recalculation of dose with modified contours.

Dose calculation

The CBCT dose calculation has been discussed earlier by several authors.[23,38-44] Yang *et al*.[16] stated that the dose difference (DD) in simple geometry was about 3% in Catphan phantom and 2% in patient images when pencil beam convolution (PBC) was used for dose calculation. However, PBC algorithm can overestimate dose in inhomogeneous region. Small changes in HU between CBCT and FBCT resulted in large dose differences when PBC was used.[45] In our study, AAA was used for dose calculation in simple geometry as well as in IMRT. Dose difference in simple geometry was <1.5% and 1.2% for IMRT (phantom and patient) cases except in build-up regions. Ding *et al*.[17] showed the dose deviation between FBCT and CBCT was <1%, even though the HU value difference was higher between the modalities. In our work, the HU changes were minimal in the central region (<20), and in the peripheral region, the difference was higher (<40HU). In the build-up region, the DD was high between FBCT based and CBCT based plans. Dose computation was not perfect in the build-up region due to algorithm limitation. Apart from that, the HU values in CBCT were not closer to their real HU values of the material which can lead to dose calculation inaccuracy. CBCT images can be used for recalculation but delineating target and normal structures are difficult and further work has to be performed.

Conclusion

This feasibility study investigated HU variation and dose calculation accuracy between FBCT and CBCT-based planning and has validated inverse planning algorithms with CBCT. Our study showed that, at the edges of the phantom, there was a larger deviation of HU values compared to the center due to the ring artifact and scatter and this may prevent the use of CBCT as the primary imaging modality for radiotherapy treatment planning. The reconstruction algorithms need to be modified further for improving the image quality and accuracy in HU values. However, our study with TG-119 test targets showed that CBCT could be used for adaptive replanning as the recalculation of the dose with the AAA algorithm was in full accord with conventional planning CT except in the build-up regions. The CBCT images have to be carefully analyzed for any artifacts before being used for dose calculations.

Conflicts of interest

There are no conflicts of interest.

References

1. Miracle AC, Mukherji SK. Conebeam CT of the head and neck, part 1: Physical principles. AJNR Am J Neuroradiol 2009;30:1088-95.
2. Jaffray DA, Siewerdsen JH, Wong JW, Martinez AA. Flat-panel cone-beam computed tomography for image-guided radiation therapy. Int J Radiat Oncol Biol Phys 2002;53:1337-49.
3. Moore CJ, Amer A, Marchant T, Sykes JR, Davies J, Stratford J, *et al.* Developments in and experience of kilovoltage X-ray cone beam image-guided radiotherapy. Br J Radiol 2006;79 Spec No 1:S66-78.
4. van-Prooijen M, Islam M, Tsui G, Laperriere N. Determination of treatment margin for the cbct-based intracranial stereotactic radiosurgery/radiotherapy. Radiother Oncol 2007;69:S683.
5. Song W, Schaly B, Bauman G, Battista J, Van Dyk J. Image-guided adaptive radiation therapy (IGART): Radiobiological and dose escalation considerations for localized carcinoma of the prostate. Med Phys 2005;32:2193-203.
6. Xu F, Wang J, Bai S, Li Y, Shen Y, Zhong R, *et al.* Detection of intrafractional tumour position error in radiotherapy utilizing cone beam computed tomography. Radiother Oncol 2008;89:311-9.
7. Barker JL Jr., Garden AS, Ang KK, O'Daniel JC, Wang H, Court LE, *et al.* Quantification of volumetric and geometric changes occurring during fractionated radiotherapy for head-and-neck cancer using an integrated CT/linear accelerator system. Int J Radiat Oncol Biol Phys 2004;59:960-70.
8. Hansen EK, Bucci MK, Quivey JM, Weinberg V, Xia P. Repeat CT imaging and replanning during the course of IMRT for head-and-neck cancer. Int J Radiat Oncol Biol Phys 2006;64:355-62.
9. Ping HS, Kandaiya S. The influence of the patient size and geometry on cone beam-computed tomography hounsfield unit. J Med Phys 2012;37:155-8.
10. Mao W, Rozario T, Lu W, Gu X, Yan Y, *et al.* Online dosimetric evaluation of larynx SBRT: A pilot study to assess the necessity of adaptive replanning. J Appl Clin Med Phys 2017;18:157-63.
11. Boggula R, Lorenz F, Abo-Madyan Y, Lohr F, Wolff D, Boda-Heggemann J, *et al.* A new strategy for online adaptive prostate radiotherapy based on cone-beam CT. Z Med Phys 2009;19:264-76.
12. Søvik A, Rødal J, Skogmo HK, Lervåg C, Eilertsen K, Malinen E. Adaptive radiotherapy based on contrast enhanced cone beam CT imaging. Acta Oncol 2010;49:972-7.
13. Bertelsen A, Schytte T, Bentzen SM, Hansen O, Nielsen M, Brink C. Radiation dose response of normal lung assessed by Cone Beam CT - A potential tool for biologically adaptive radiation therapy. Radiother Oncol 2011;100:351-5.
14. Kibrom AZ, Knight KA. Adaptive radiation therapy for bladder cancer: A review of adaptive techniques used in clinical practice. J Med Radiat Sci 2015;62:277-85.
15. Zhang GS, Huang SM, Chen C, Xu SK, Zhang DD, Deng XW. Evaluating the therapeutic dose distribution of intensity-modulated radiation therapy for head and neck with cone-beam computed tomography image: A methodological study. Biomed Res Int 2014;2014:326532.
16. Yang Y, Schreibmann E, Li T, Wang C, Xing L. Evaluation of on-board kV cone beam CT (CBCT)-based dose calculation. Phys Med Biol 2007;52:685-705.
17. Ding GX, Duggan DM, Coffey CW, Deeley M, Hallahan DE, Cmelak A, *et al.* A study on adaptive IMRT treatment planning using kV cone-beam CT. Radiother Oncol 2007;85:116-25.
18. Ezzell GA, Burmeister JW, Dogan N, LoSasso TJ, Mechalakos JG,

Mihailidis D, *et al.* IMRT commissioning: Multiple institution planning and dosimetry comparisons, a report from AAPM Task Group 119. Med Phys 2009;36:5359-73.

19. Ezzell GA. Clinical Implementation of IMRT Treatment Planning AAPM Summer School Proceedings; 2003. p. 475-92.

20. Feldkamp LA, Davis L, Kress J. Practical cone-beam algorithm. J Opt Soc Am 1984;1:612-9.

21. Yoo S, Kim GY, Hammoud R, Elder E, Pawlicki T, Guan H, *et al.* A quality assurance program for the on-board imagers. Med Phys 2006;33:4431-47.

22. Catphan® 500 and 600 Manual. Salem, NY: The Phantom Laboratory.

23. Hatton J, McCurdy B, Greer PB. Cone beam computerized tomography: The effect of calibration of the Hounsfield unit number to electron density on dose calculation accuracy for adaptive radiation therapy. Phys Med Biol 2009;54:N329-46.

24. Thomas SJ. Relative electron density calibration of CT scanners for radiotherapy treatment planning. Br J Radiol 1999;72:781-6.

25. Chung H, Jin H, Palta J, Suh TS, Kim S. Dose variations with varying calculation grid size in head and neck IMRT. Phys Med Biol 2006;51:4841-56.

26. ICRU Report 83 Prescribing, Recording and Reporting Photon-Beam Intensity-Modulated Radiation Therapy (IMRT); 2010.

27. ICRU Report 42 Use of Computers in External Beam Radiotherapy Procedures with High Energy Photons and Electrons; 1987.

28. Men K, Dai J, Chen X, Li M, Zhang K, Huang P. Dual-energy imaging method to improve the image quality and the accuracy of dose calculation for cone-beam computed tomography. Phys Med 2017;36:110-118.

29. Gardner SJ, Studenski MT, Giaddui T, Cui Y, Galvin J, Yu Y, *et al.* Investigation into image quality and dose for different patient geometries with multiple cone-beam CT systems. Med Phys 2014;41:031908.

30. Stanley DN, Papanikolaou N, Gutiérrez AN. An evaluation of the stability of image-quality parameters of Varian on-board imaging (OBI) and EPID imaging systems. J Appl Clin Med Phys 2015;16:87-98.

31. Kurz C, Kamp F, Park YK, Zöllner C, Rit S, Hansen D, *et al.* Investigating deformable image registration and scatter correction for CBCT-based dose calculation in adaptive IMPT. Med Phys 2016;43:5635.

32. Elstrøm UV, Wysocka BA, Muren LP, Petersen JB, Grau C. Daily kV cone-beam CT and deformable image registration as a method for studying dosimetric consequences of anatomic changes in adaptive IMRT of head and neck cancer. Acta Oncol 2010;49:1101-8.

33. Dunlop A, McQuaid D, Nill S, Murray J, Poludniowski G, Hansen VN, *et al.* Comparison of CT number calibration techniques for CBCT-based dose calculation. Strahlenther Onkol 2015;191:970-8.

34. Jin JY, Ren L, Liu Q, Kim J, Wen N, Guan H, *et al.* Combining scatter reduction and correction to improve image quality in cone-beam computed tomography (CBCT). Med Phys 2010;37:5634-44.

35. Niu K, Tang J, Royalty V, Ozkan O, Strother C, Aagaard-Kienitz B, *et al.* Radiation Dose Reduction and CNR Enhancement in C-Arm Cone Beam CT Medical Imaging, Vol. 8668. Physics of Medical Imaging, Proceedings of SPIE; 2013. p. 2S, 1-6.

36. Wang AS, Stayman JW, Otake Y, Kleinszig G, Vogt S, Gallia GL, *et al.* Soft-tissue imaging with C-arm cone-beam CT using statistical reconstruction. Phys Med Biol 2014;59:1005-26.

37. Altunbas C, Lai CJ, Zhong Y, Shaw CC. Reduction of ring artifacts in CBCT: Detection and correction of pixel gain variations in flat panel detectors. Med Phys 2014;41:091913.

38. Rong Y, Smilowitz J, Tewatia D, Tomé WA, Paliwal B. Dose calculation on kV cone beam CT images: An investigation of the Hu-density conversion stability and dose accuracy using the site-specific calibration. Med Dosim 2010;35:195-207.

39. Guan H, Dong H. Dose calculation accuracy using cone-beam CT (CBCT) for pelvic adaptive radiotherapy. Phys Med Biol 2009;54:6239-50.

40. Zhang Y, Yin FF, Ren L. Dosimetric verification of lung cancer treatment using the CBCTs estimated from limited-angle on-board projections. Med Phys 2015;42:4783-95.

41. Jin X, Hu W, Shang H, Han C, Yi J, Zhou Y, *et al.* CBCT-based volumetric and dosimetric variation evaluation of volumetric modulated arc radiotherapy in the treatment of nasopharyngeal cancer patients. Radiat Oncol 2013;8:279.

42. Wang J, Hu W, Cai G, Peng J, Pan Z, Guo X, *et al.* Using corrected cone-beam CT image for accelerated partial breast irradiation treatment dose verification: The preliminary experience. Radiat Oncol 2013;8:214.

43. Kurz C, Dedes G, Resch A, Reiner M, Ganswindt U, *et al.* Comparing cone-beam CT intensity correction methods for dose recalculation in adaptive intensity-modulated photon and proton therapy for head and neck cancer. Acta Oncol 2015;54:1651-7.

44. Veiga C, McClelland J, Moinuddin S, Lourenço A, Ricketts K, Annkah J, *et al.* Toward adaptive radiotherapy for head and neck patients: Feasibility study on using CT-to-CBCT deformable registration for "dose of the day" calculations. Med Phys 2014;41:031703.

45. Fogliata A, Vanetti E, Albers D, Brink C, Clivio A, Knöös T, *et al.* On the dosimetric behaviour of photon dose calculation algorithms in the presence of simple geometric heterogeneities: Comparison with Monte Carlo calculations. Phys Med Biol 2007;52:1363-85.